JOURNAL OF MARITIME RESEARCH

Vol XXII. No. III (2025) pp 74–82

**ISSN: 1697-4840, www.jmr.unican.es**

# Influence of Rebar Configuration and Reservoir Size on Corrosion Dynamics in Fly Ash Concrete: A Galvanostatic Pulse Study

Kazi Naimul Hoque[1,*], Francisco Presuel-Moreno[2]

*ARTICLE INFO*

***Article history:***
Received 22 Nov 2024;
in revised from 23 Dec 2024;
accepted 18 Mar 2025.

***Keywords:***
Fly ash, reservoir length, galvanostatic pulse measurements, corrosion current, corrosion potential, concrete solution resistance.

*ABSTRACT*

This study investigates corrosion propagation in fly ash (FA) concrete with single rebar and three rebars, prepared using a w/cm ratio of 0.41. Accelerated chloride transport was achieved through electromigration approach. Corrosion initiation was detected at a rebar potential of -150 mV vs. saturated calomel electrode (SCE), while propagation was evaluated using galvanostatic pulse (GP) measurements. Throughout 300–1600 days, the size of the reservoir had a notable impact on corrosion current behavior. The larger reservoirs showed a steady decrease in corrosion current values, while smaller reservoirs had lower but more variable corrosion current values. The intermediate reservoirs (7.5 cm) showed the highest corrosion activity among the single rebar samples, likely due to balanced oxygen and moisture levels. The three rebar samples experienced higher corrosion currents, more negative potentials, and greater susceptibility to corrosion. The renewed corrosion activity on some selected samples after 1400 days suggests passive layer breakdown, highlighting the role of reservoir size, rebar configuration, and environmental factors in FA concrete durability.



## 1. Introduction.

Steel reinforcement within concrete benefits from a naturally protective oxide layer due to the material's highly alkaline environment (pH~13). This passive layer significantly inhibits corrosion. However, corrosion of steel rebar remains the most prevalent durability issue for reinforced concrete. Chloride ion penetration to the steel surface is recognized as the primary trigger for corrosion initiation in rebar [1–4]. The corrosion-induced damage in reinforced concrete manifests in two significant ways. First, the steel rebar's cross-sectional area diminishes due to material loss. Second, the corrosion process generates expansive products, which occupy greater volume than the original steel. This expansion induces tensile stresses in the surrounding concrete, leading to cracking, spalling, and ultimately, structural failure [5–10].

To address these issues, fly ash has been increasingly used as a partial replacement for cement. During hydration, fly ash reacts with calcium hydroxide to form secondary compounds, which significantly reduce the porosity of the concrete matrix [11]. The fine granules of fly ash obstruct pores and voids, reducing pore size and limiting the diffusion of chloride ions and other corrosive agents. This densification effect is hypothesized to enhance concrete resistivity.

Accelerated corrosion testing is widely used to model steel corrosion in reinforced concrete (RC) structures. Such tests simulate corrosion mechanisms and evaluate damage, including loss of steel-concrete bond, surface cracking, spalling, and structural stiffness reduction. The need for advanced research is emphasized to better simulate natural corrosion propagation and minimize associated damage, particularly by extending the initiation phase of corrosion.

In this study, 20% of ordinary Portland cement was replaced with fly ash in the concrete mix. The length of the anode was adjusted by modifying the size of the solution reservoir, and the

[1]Department of Naval Architecture and Marine Engineering, Bangladesh University of Engineering and Technology (BUET), Dhaka-1000, Bangladesh.
[2]Department of Ocean and Mechanical Engineering, Florida Atlantic University (FAU), Dania Beach, Florida-33004, USA.
[*]Corresponding author: Kazi Naimul Hoque. E-mail Address: kazinaim@name.buet.ac.bd.

accelerated chloride transport technique was employed to expedite chloride ingress by means of electromigration approach. This experimental approach was developed based on insights from previous studies [12]. Corrosion typically initiated within weeks to months. Throughout approximately 1600 days of corrosion propagation, parameters like corrosion current, corrosion potential, and concrete solution resistance were monitored using galvanostatic pulse (GP) measurements.

## 2. Experimental Details.

In April 2016, reinforced concrete specimens incorporating a binary mix with fly ash (FA) were prepared, utilizing a w/cm ratio of 0.41. Detailed specifications of the mix are provided in Table 1 and in reference [13]. The rebar segments were sized appropriately and cleaned with hexane to remove grease before casting, following wire-brushing. The specimens were fabricated in two dimensions: $30.0 \times 12.7 \times 7.6$ cm for single rebar sections and $30.0 \times 30.0 \times 7.6$ cm for three rebar sections. The single rebar samples had a radius of 0.47 cm, while three rebar specimens featured with a radius of 0.63 cm. A total of eleven specimens with single rebar and twelve specimens with three rebars were prepared, incorporating concrete covers of 1.9 cm and 2.5 cm. To facilitate corrosion monitoring, the rebars were drilled and tapped for electrical contact. All specimens included stainless steel mesh or titanium mixed metal oxide (TiMMO) mesh embedded along the casting surface, which was later used as the bottom

Table 1: Concrete mix specifications for FA specimens.

| Mix | Cast Date | Cementitious Content ($kg/m^3$) | Cement Content ($kg/m^3$) | 20% FA ($kg/m^3$) | Fine agg. ($kg/m^3$) | Coarse agg. ($kg/m^3$) | w/cm ratio |
|---|---|---|---|---|---|---|---|
| FA | 4/18/2016 | 390 | 312 | 78 | 967 | 833 | 0.41 |

Source: Authors.

The specimens were initially prepared at the State Materials Office of the Florida Department of Transportation (FDOT-SMO). After 24 hours, the molds were removed, and the samples were cured in a fog room at high humidity for approximately one month. By the end of May 2016, they were transferred to the FAU SeaTech campus. There, the samples were stored in a high-humidity environment until solution reservoirs were installed on the casting surface, roughly 40 days after casting. These reservoirs, attached with marine-grade adhesives, were filled with a 10% by weight NaCl solution to initiate corrosion. To constrain the corrosion-affected region, the reservoir lengths were adjusted. Prior to filling the reservoirs, the samples were pre-conditioned in high-humidity environments for 3–7 days. Electrodes matching the dimensions of the embedded meshes were placed on the reservoir's top surface. Additionally, the bottom 1 cm of each sample was immersed in a saturated calcium hydroxide solution to minimize leaching, with a perforated acrylic mesh overlay applied as a protective measure.

## 3. Accelerated Chloride Transport.

A controlled electrical potential was applied across the specimens using a power supply to facilitate chloride ingress into the concrete. The electric field generated between the top and bottom mesh, drove the chlorides from the NaCl solution toward the embedded rebar. The electrode submerged in the NaCl solution was connected to the negative terminal of the power source, while the embedded mesh within each specimen was linked to the positive terminal. To prevent direct contact between the TiMMO mesh and the concrete, an acrylic mesh was added to the solution reservoir. The experimental setup for this accelerated chloride transport process is illustrated in Figure 1.

Table 2: Different single rebar samples made with fly ash replacement.

| Sample Number | Reservoir length (cm) | Total Ampere-Hour |
|---|---|---|
| FA-1 | 5 | 4.069 |
| FA-2 | | 3.015 |
| FA-3 | | 1.718 |
| FA-4 | 7.5 | 5.889 |
| FA-5 | | 3.524 |
| FA-6 | | 3.729 |
| FA-7 | 17.5 | 8.145 |
| FA-8 | | 6.942 |
| FA-9 | | 6.676 |
| FA-10 | 2.5 | 2.742 |
| FA-11 | | 3.531 |

Source: Authors.

Table 3: Different three rebar samples made with fly ash replacement.

| Sample Number | Reservoir length (cm) | Total Ampere-Hour |
|---|---|---|
| 5X (FA) | 2.5 | 1.493 |
| 7X (FA) | 5 | 3.262 |
| 10X (FA) | 2.5 | 3.262 |
| 11X (FA) | 2.5 | 0.758 |
| 12X (FA) | 5 | 0.758 |
| 13X (FA) | 10 | 2.269 |
| 14X (FA) | 15 | 2.304 |
| 18X (FA) | 15 | 1.484 |
| 20X (FA) | 10 | 3.320 |
| 21X (FA) | 10 | 2.410 |
| 23X (FA) | 5 | 1.407 |
| 24X (FA) | 15 | 1.598 |

Source: Authors.

Each specimen was labeled as per Tables 2 and Table 3, which provide details including sample identification, solution reservoir length, and the total calculated Ampere-hours applied. Both single rebar and three rebar specimens prepared with fly ash were characterized in Tables 2 and Table 3.

Figure 1: Experimental setup used for accelerated chloride transport method.

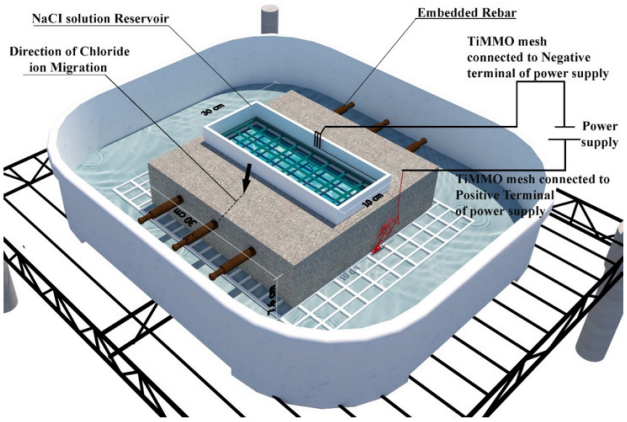


Source: Authors.

The accelerated chloride transport technique was conducted with an initial applied voltage of 9 V. Measurements of the rebar potential relative to a saturated calomel reference electrode (SCE) indicated a potential exceeding +2 V during the initial phase. After seven days, the applied voltage was reduced to 3 V to stabilize the process. The current flow through the system was monitored by measuring the voltage drop across a 100-ohm resistor, which allowed for precise current calculations over several days. Even when the system was temporarily disconnected, ionic currents generated by the applied electric field caused the rebar to remain polarized. If corrosion initiation was not detected in the final rebar potential readings (measured off-system), the applied potential was resumed. Typically, the rebar potential was monitored for up to two hours with the system disconnected. The process continued until the specimen exhibited an off-rebar potential of -150 mV vs. SCE or more negative, signaling the initiation of corrosion in the embedded rebar. This threshold potential, corresponding to approximately -220 mV vs. a copper sulfate electrode (CSE), is widely recognized as indicative of corrosion initiation [12].

## 4. Measurements for Assessing Corrosion Propagation.

To monitor rebar potential during the corrosion propagation phase following the accelerated chloride transport process, a SCE and a high-impedance voltmeter were routinely employed. Early-stage electrochemical characterization, including techniques such as linear polarization resistance (LPR) and electrochemical impedance spectroscopy (EIS), was performed, with results documented in reference [13].

Beginning in April 2017, GP tests were implemented as an alternative for determining concrete solution resistance (Rs) and polarization resistance (Rc) values. These measurements were conducted approximately once a month throughout the corrosion propagation phase. Initially, a 10 μA galvanostatic current was applied, but adjustments were made to ensure the polarization stayed below 25 mV relative to the instant-on potential (the difference between the corrosion potential measured at 0.2 seconds and the final on-potential value). The first round of GP tests lasted 140 seconds, but this duration was increased to 300 seconds in later tests, as some rebar slopes continued to change beyond the initial duration, necessitating a stable slope for accurate (Rc) calculation. Later tests adopted a duration of 200 seconds as a balanced approach.

During each test, the GP device first recorded the open-circuit potential for several seconds. After the pulse was applied, rebar potential was measured at 0.2 millisecond intervals over time. The concrete solution resistance (Rs)) was calculated using the rebar potential before the GP test and the initial on-potential under the applied pulse. The polarization resistance (Rc) was determined by comparing the initial on-potential to the rebar potential at 200 seconds, along with the applied current. The Rc values derived from GP tests were then converted into corrosion current (Icorr) values, as the exact corroding surface area was unknown. The Stern-Geary equation (Icorr= B/Rp) was used to calculate Icorr, where Rp (equivalent to Rc) represents the polarization resistance, and B is the Stern-Geary constant. The value of B ranges from 13 to 52 mV depending on whether the steel is in a passive or active corrosion state. Following established guidelines, a value of 26 mV was selected for this study to represent actively corroding steel [14–16].

## 5. Results and Discussion.

### *5.1. Evolution of Icorr with time.*

The following section illustrates the progression of Icorr over time, as measured using the GP method, for samples made with FA concrete mixes containing either single rebar or three rebars. It is important to note that day zero in most of the plots refers to the day the solution was introduced into the solution reservoir, rather than the specimen's age. Since the reservoirs were not all installed simultaneously, the number of days since the initial filling varies between samples. The Icorr readings for all samples was recorded using the GP method, covering the period from day 300 to day 1600.

Figure 2 illustrates the evolution of Icorr over time for FA concrete samples embedded with single rebars, measured under different solution reservoir sizes using the GP method. For the 17.5 cm reservoir size, most samples exhibit a general decline in Icorr over time. However, the FA-8 sample shows a steady, monotonic decrease throughout the testing period. Both FA-8 and FA-9 samples were terminated at around 620 days, with Icorr values ranging from 6.4 to 22.1 $\mu$A. In the 7.5 cm reservoir size, all samples initially show a downward trend in Icorr until around 1160 days, after which the trends become more erratic. Over this period, Icorr values range between 6.1 and 39.5 $\mu$A. Notably, FA-4 and FA-6 exhibit an increase in Icorr between 1100 and 1200 days, followed by a decline when placed in an

Figure 2: Icorr with time obtained from GP method on selected rebars (FA samples) under different size reservoir.

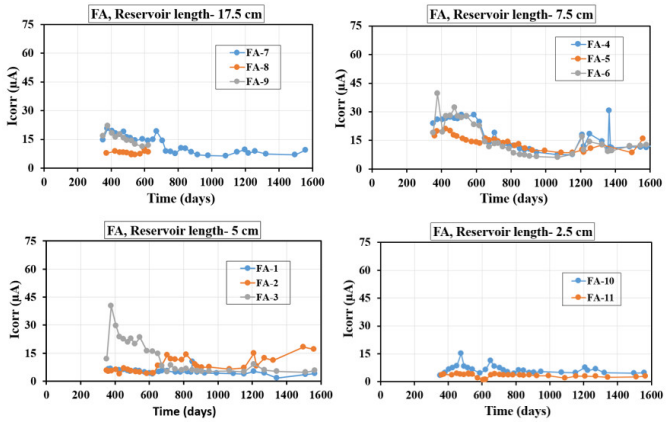


Source: Authors.

environmental chamber. After this point, both specimens show a gradual, monotonic rise. For the 5 cm reservoir size, most samples exhibit fluctuating Icorr trends over time. An exception is FA-1 sample, which remains largely stable, showing a plateau trend. The FA-2 sample, however, displays a rise in Icorr during the last 400 days. In general, the Icorr values for samples with a 5 cm reservoir size vary between 1.7 and 40.2 $\mu$A. Regarding the 2.5 cm reservoir size, FA-10 demonstrates fluctuating Icorr values, while FA-11 follows a predominantly monotonic decrease. The Icorr values for this reservoir size vary between 1.0 and 15.2 $\mu$A. When comparing reservoir sizes, samples with a 7.5 cm reservoir generally exhibit the highest Icorr values. Specimens with 5 cm and 17.5 cm reservoirs show similar Icorr magnitudes, while the 2.5 cm reservoir results in the lowest corrosion currents. Furthermore, for specific samples, Icorr values are comparable between the 5 cm and 7.5 cm reservoirs, as well as between the 2.5 cm and 5 cm reservoirs.

Figure 3: Icorr with time obtained from GP method for three rebar FA samples under 15 cm solution reservoir.

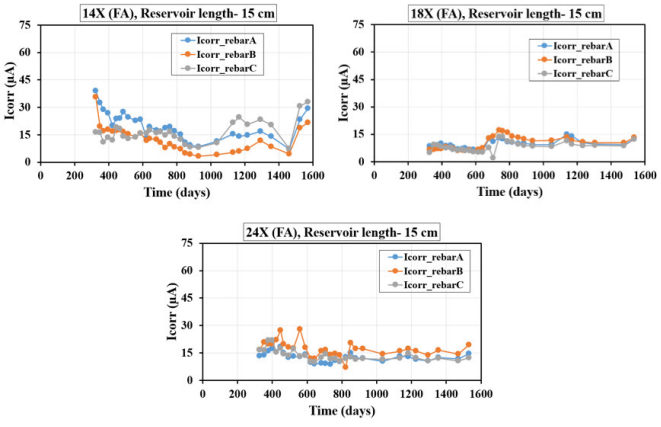


Source: Authors.

Figure 3 presents the Icorr measurements for three rebars (A, B, and C) over roughly 1600 days, using a solution reservoir length of 15 cm. Each plot represents a different experimental condition, indicated by 14X, 18X, and 24X labels. In the case of 14X sample, initially, Icorr is high for all rebars, indicating active corrosion, but it decreases after around 400 days. From about 500 to 1100 days, the corrosion current for rebars A and B remains relatively low but gradually increases towards 1100 days. After 1100 days, the corrosion current stabilizes with slight fluctuations but rises significantly after 1400 days, reaching values around 30 $\mu$A for rebar A and around 20–35 $\mu$A for rebar B and C. For the plot in case of 18X sample, Icorr is initially lower than in the 14X plot, with values below 10 $\mu$A. It spikes around 750 days for all rebars and then settles around 10–20 $\mu$A. Between 800 and 1400 days, the corrosion current remains stable with minimal fluctuations. After 1400 days, a slight increase is observed for all rebars, indicating a potential increase in corrosion activity. For 24X sample, the Icorr shows frequent spikes, particularly for rebar B, which has higher values at various points (especially around 450 and 550 days). After 800 days, the current stabilizes but fluctuates slightly around 10–20 $\mu$A. Similar to the other plots, there is an increase after 1400 days, but the values are lower than those of 14X. Each plot begins with a period of high corrosion activity, which declines over time. A relatively stable phase occurs after 800 days, with moderate Icorr values. All configurations show an increase in Icorr after 1400 days, suggesting possible renewed corrosion activity or environmental changes affecting corrosion. This data suggests variations in rebar corrosion behavior potentially due to differences in oxygen availability, moisture content, temperature, or other environmental factors affecting each setup.

Figure 4: Icorr with time obtained from GP method for three rebar FA samples under 2.5 cm solution reservoir.

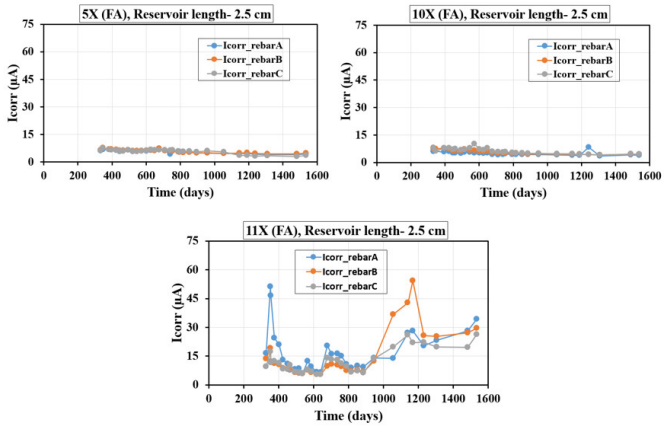


Source: Authors.

The three plots in Figure 4 show the variation of Icorr with time for three rebars (A, B, and C) subjected to a constant solution reservoir length of 2.5 cm. In case of 5X sample, the corrosion currents for rebars A, B, and C remain relatively stable over time, staying below 10 $\mu$A. The minimal fluctuations are observed, indicating stable passive conditions or low levels of corrosion. The corrosion rates appear consistent for all three rebars, suggesting uniform environmental exposure. For

the case of 10X sample, corrosion currents continue to exhibit low and stable trends, with values staying below approximately 5 $\mu$A for most of the timeline. A small spike in corrosion current is observed for rebar A near 1300 days, but it quickly returns to baseline. Similar to the first plot, the overall corrosion remains low and controlled across the rebars. While considering 11X sample, significant variation is evident in this plot compared to the first two plots. The corrosion current for rebar B rises sharply around 1150 days, reaching nearly 60 $\mu$A. This suggests an increase in corrosion activity, possibly due to changes in the environment or material properties. Rebar A also shows a noticeable increase in corrosion current after 1000 days, peaking at around 35 $\mu$A towards the end. Rebar C exhibits a smaller increase in corrosion current compared to rebar A and rebar B, but still shows notable variation. The trends suggest that the passive layer might have been compromised after extended exposure, leading to accelerated corrosion for some rebars. The progression from 5X to 11X sample reveals an increasing tendency for corrosion activity over time, especially after 1000 days. The initial conditions suggest uniform and stable corrosion behavior; however, external factors or changes in material properties may have triggered non-uniform corrosion in later stages. The sharp increase in Icorr in the 11X sample suggests the need for further investigation into the protective mechanisms of rebars and their breakdown over time. The results for the remaining three rebar FA samples are available in references [13, 17, 18].

Tables 4 and Table 5 summarize the Icorr average and standard deviation (STD) values obtained from measurements performed between day 300 and day 1600, covering the latest 15 data sets. These readings were acquired using the GP method and pertain to FA concrete specimens with both single rebar and three rebar configurations.

Table 4 focuses on Icorr averages and STD values for FA specimens with single rebar, based on GP measurements. For a reservoir length of 17.5 cm, the FA-7 specimen showed an Icorr average of 8.2 $\mu$A and an STD of 1.4 $\mu$A. Meanwhile, FA-8 and FA-9 were excluded as they were terminated before data collection. For specimens with a 7.5 cm reservoir length, the Icorr averages and STDs for FA-4, FA-5, and FA-6 were 12.6 $\mu$A, 11.0 $\mu$A, and 10.0 $\mu$A, with corresponding STDs of 5.2 $\mu$A, 2.3 $\mu$A, and 2.9 $\mu$A. Samples with a reservoir length of 5 cm, namely FA-1, FA-2, and FA-3, recorded Icorr averages of 4.6 $\mu$A, 10.9 $\mu$A, and 5.7 $\mu$A, with STDs of 2.0 $\mu$A, 3.9 $\mu$A, and 1.1 $\mu$A, respectively. Similarly, the 2.5 cm reservoir length samples, FA-10 and FA-11, had Icorr averages of 5.5 $\mu$A and 3.0 $\mu$A, with STDs of 0.9 $\mu$A and 0.5 $\mu$A, respectively. It is interesting to note that the highest Icorr average was observed in FA-4 sample, associated with a reservoir length of 7.5 cm, while the lowest was recorded in FA-11 sample, corresponding to a reservoir length of 2.5 cm. The Icorr averages across the FA specimens with varying reservoir lengths were found to be comparable, highlighting the impact of reservoir size on the corrosion behavior of embedded rebars. The Icorr average values for FA samples were reported as 49.9 $\mu$A [19], and 17.6 $\mu$A [20] respectively.

Table 4: Icorr average and STD obtained from GP readings for FA single rebar specimens.

| Sample Number | Reservoir length (cm) | Icorr avg. (µA) | STD (µA) |
|---|---|---|---|
| FA-1 | 5 | 4.6 | 2.0 |
| FA-2 | | 10.9 | 3.9 |
| FA-3 | | 5.7 | 1.1 |
| FA-4 | 7.5 | 12.6 | 5.2 |
| FA-5 | | 11.0 | 2.3 |
| FA-6 | | 10.0 | 2.9 |
| FA-7 | 17.5 | 8.2 | 1.4 |
| FA-8* | | - | - |
| FA-9* | | - | - |
| FA-10 | 2.5 | 5.5 | 0.9 |
| FA-11 | | 3.0 | 0.5 |

Note: (*) stands for those specimens that have been terminated.
Source: Authors.

Table 5 provides the Icorr average and STD values obtained from GP measurements for FA specimens with three rebars. Among these, the highest Icorr average of 22.5 $\mu$A was recorded for 11X-B, with an STD of 15.6 $\mu$A. For the other rebars in the 11X series, 11X-A and 11X-C, the Icorr averages were 18.7 $\mu$A and 16.2 $\mu$A, with corresponding STDs of 8.7 $\mu$A and 7.4 $\mu$A. This 11X sample featured a reservoir length of 2.5 cm. Conversely, the lowest Icorr average of 4.5 $\mu$A was observed in 10X-A, with an STD of 1.2 $\mu$A. The Icorr averages for the other rebars in the 10X series, 10X-B and 10X-C, were slightly higher at 4.6 $\mu$A and 4.8 $\mu$A, with respective STDs of 0.3 $\mu$A and 0.5 $\mu$A. The 10X sample also had a reservoir length of 2.5 cm. Interestingly, both the highest and lowest Icorr averages for the FA three rebar specimens were associated with the smallest reservoir length of 2.5 cm. A notable range of Icorr average and STD values was observed across different FA three rebar specimens. Additionally, Icorr averages were comparable for selected rebars within FA specimens across varying reservoir lengths, providing valuable insights into corrosion behavior under different conditions.

Table 5: Icorr average and STD obtained from GP readings for FA three rebar specimens.

| Sample Number | Reservoir length (cm) | Rebar Number | | | | | |
|---|---|---|---|---|---|---|---|
| | | A | | B | | C | |
| | | Icorr avg. (µA) | STD (µA) | Icorr avg. (µA) | STD (µA) | Icorr avg. (µA) | STD (µA) |
| 5X (FA) | 2.5 | 4.9 | 0.6 | 5.0 | 0.4 | 4.8 | 1.3 |
| 10X (FA) | | 4.5 | 1.2 | 4.6 | 0.3 | 4.8 | 0.5 |
| 11X (FA) | | 18.7 | 8.7 | 22.5 | 15.6 | 16.2 | 7.4 |
| 7X (FA) | 5 | 6.0 | 1.1 | 6.6 | 1.3 | 6.1 | 0.5 |
| 12X (FA) | | 19.0 | 7.9 | 22.2 | 7.1 | 21.7 | 5.9 |
| 23X (FA) | | 11.0 | 2.1 | 9.4 | 2.6 | 12.2 | 1.9 |
| 13X (FA) | 10 | 8.5 | 3.1 | 9.4 | 2.8 | 6.2 | 1.4 |
| 20X (FA) | | 7.9 | 3.4 | 8.7 | 3.9 | 11.4 | 6.8 |
| 21X (FA) | | 11.6 | 4.7 | 12.8 | 6.3 | 12.9 | 6.3 |
| 14X (FA) | 15 | 14.1 | 4.4 | 7.5 | 4.1 | 16.3 | 7.3 |
| 18X (FA) | | 11.0 | 1.9 | 12.7 | 2.0 | 10.0 | 1.7 |
| 24X (FA) | | 12.2 | 1.4 | 15.7 | 3.2 | 12.0 | 1.1 |

Source: Authors.

### 5.2. *Ecorr (corrosion potential) vs. Icorr (corrosion current).*

Figure 5 presents Ecorr vs. Icorr plots derived from GP readings for FA concrete specimens containing single rebar and three rebars. This plot was developed using data from the two most recent measurement sets. In the plot, solid-filled points represent samples with three rebars, while unfilled points represent samples with a single rebar.

A significant scatter in Ecorr and Icorr values was observed across all FA samples, as shown in Figure 5. The Ecorr values ranged from -439.1 mV to -46.4 mV, while Icorr spanned from 2.7 μA to 31.2 μA. Notably, several rebars displayed Ecorr values more negative than -300 mV (Ecorr ≤ -300 mVsce) alongside high Icorr values, indicative of active corrosion. Many other rebars fell within an intermediate potential range of -300 mV to -100 mV, and only a few exhibited more positive potentials exceeding -100 mV. The shift toward more positive Ecorr values in some rebars could be attributed to localized re - passivation of corroding sites or polarization effects from non - corroding regions over time. This suggests that corrosion dynamics may involve both active and passive states depending on the rebar environment and interaction with the surrounding concrete matrix. Interestingly, the Ecorr values for three rebar FA samples were generally more negative compared to single rebar FA specimens, indicating a potentially higher tendency for corrosion in three rebar systems. Additionally, many rebars recorded Icorr values exceeding 10.0 μA, further reinforcing the observation of active corrosion in certain cases. Figure 5 further emphasizes a notable difference in the slopes derived from the FA specimen readings for single rebar and three rebar configurations. This variation in slope indicates potential differences in the underlying corrosion mechanisms or the environmental factors influencing the specimens. The difference may arise due to variations in rebar diameters, as the larger combined surface area in three rebar specimens could lead to distinct electrochemical interactions compared to single rebar specimens. These interactions might affect the distribution of corrosion sites, polarization behavior, or the ability of the surrounding concrete matrix to protect the embedded rebars. Similar observations were found in these studies [21–25].

### 5.3. *Icorr (corrosion current) vs. Rs (concrete solution resistance).*

Figure 6 and Figure 7 illustrate the relationship between Icorr and Rs for FA concrete mixes embedded with either a single rebar or three rebars, as derived from GP measurements. Each figure includes two plots: the left plot represents the initial Icorr vs. Rs values obtained during the initial GP measurements (the first three readings), while the right plot shows the most recent data (the latest two readings).

In Figure 6, focusing on FA concrete samples with a single rebar, the Rs values for rebars beneath the 2.5 cm reservoir size are consistently higher than those observed for other reservoir sizes, both initially and in the later measurements. However, the recent Rs values for these samples exhibit a significant increase compared to their initial Rs values. For rebars under the 5 cm reservoir size, a broader range of Icorr values is evident compared to other reservoir sizes. Interestingly, the recent Icorr for

Figure 5: Ecorr vs. Icorr plot for FA samples cast with single rebar and three rebars.

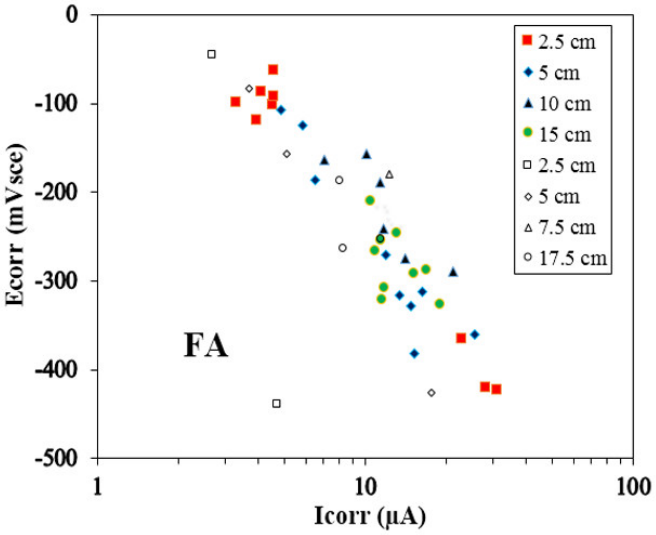


Source: Authors.

rebars under the 5 cm reservoir is similar to the values for the 7.5 cm reservoir size. Likewise, the recent Icorr values for the 7.5 cm reservoir closely resemble those of the 17.5 cm reservoir size. This suggests that the corrosion active area beneath these reservoir sizes might be comparable, as indicated by the similarity in corrosion currents. Additionally, while Rs values for the 7.5 cm reservoir samples align closely with those of the 17.5 cm samples, the Icorr values (both initial and recent) for the 7.5 cm reservoir size are notably higher. This indicates that despite similar resistances, the corrosion activity is more pronounced for the 7.5 cm reservoir samples.

Figure 6: Icorr vs. Rs plot for FA single rebar samples.

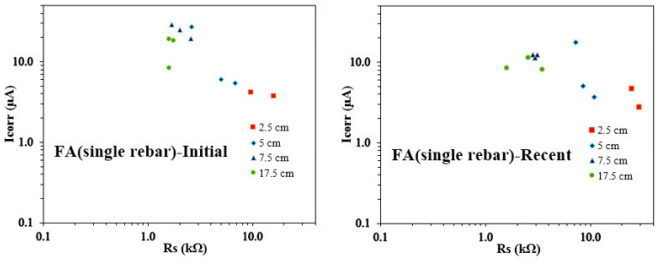


Source: Authors.

Figure 7 presents the relationship between the Icorr and Rs for FA concrete samples containing three rebars. Across all reservoir sizes, the recent Rs values are noticeably higher compared to their initial measurements. Among these, the 15 cm reservoir size consistently exhibits the smallest Rs values, both initially and in the most recent readings. It is interesting to note that in some cases, the initial and recent Icorr values for rebars under different reservoir sizes are similar. This similarity implies that the actively corroding regions beneath the reservoirs may have comparable areas. A closer inspection reveals that the

initial Icorr values are higher for the 10 cm and 15 cm reservoir sizes, whereas the recent Icorr values peak for the 15 cm reservoir size. Moreover, the Icorr vs. Rs data for rebars under the 15 cm reservoir size is more clustered in the recent measurements, suggesting a consistent corrosion pattern. Conversely, the data for the 2.5 cm, 5 cm, and 10 cm reservoir sizes exhibit greater variability, with more dispersed Icorr and Rs values in the recent readings. This spread indicates differing corrosion behaviors across these reservoir sizes. A comparable finding has been documented in studies [26–28].

Figure 7: Icorr vs. Rs plot for FA single rebar samples.

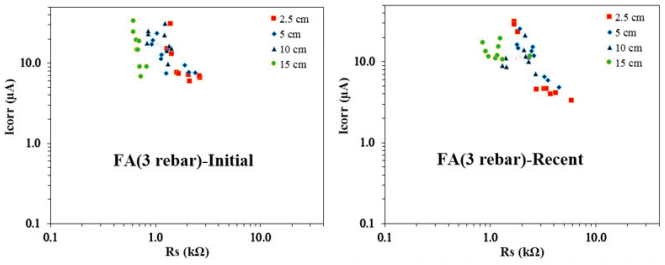


Source: Authors.

## 6. General Discussion.

The results obtained from the GP method provide valuable insights into the corrosion behavior of FA concrete specimens containing either single or three rebars. The analysis of Icorr evolution with time, Ecorr variation with Icorr, and Icorr dependency on Rs highlights critical differences in the behavior of these configurations and the influence of reservoir size on corrosion dynamics.

The evolution of Icorr demonstrates the significant role of reservoir size and rebar configuration in influencing corrosion behavior. The larger reservoirs (17.5 cm) in single rebar samples show declining Icorr trends, suggesting stabilization, while smaller reservoirs (2.5 cm) produce lower but more variable Icorr values due to limited oxygen and electrolyte availability. Interestingly, a 7.5 cm reservoir promotes higher Icorr, likely from optimal moisture and oxygen balance. For three rebar specimens, Icorr trends show greater fluctuations, with initial stabilization disrupted by spikes after 1400 days, likely due to environmental changes or passive layer degradation. These findings highlight the complex interplay between environmental factors and rebar configurations in corrosion dynamics.

The Ecorr vs. Icorr relationship highlights distinct electrochemical behaviors influenced by rebar configuration. Single rebar specimens occasionally exhibit more positive Ecorr values, indicating localized re-passivation and less aggressive corrosion conditions, with lower Icorr generally correlating to reduced corrosion rates. In contrast, three rebar specimens display more negative Ecorr values and higher Icorr, often exceeding 10 $\mu$A, reflecting increased susceptibility to active corrosion due to greater cathodic activity and electrochemical interactions among rebars. The variation in slopes between single and three rebar systems underscores the impact of configuration on anodic and cathodic dynamics, with three rebar setups promoting localized anodic dissolution [29].

The Icorr vs. Rs relationship demonstrates the influence of reservoir size and configuration on corrosion behavior. For single rebar specimens, Rs increases with decreasing reservoir size due to reduced ionic conductivity. Smaller reservoirs (e.g., 2.5 cm) exhibit higher Rs but relatively low Icorr, indicating limited corrosion kinetics due to restricted electrolyte volume. In contrast, mid-sized reservoirs (e.g., 7.5 cm) show elevated Icorr, likely due to optimal oxygen diffusion and electrolyte availability. The three rebar specimens follow similar Rs trends, with higher Rs for smaller reservoirs. However, data clustering for the 15 cm reservoir suggests a more consistent corrosion pattern, while smaller reservoirs exhibit greater variability. Over time, increased Rs in three rebar systems coincides with Icorr spikes, highlighting persistent localized corrosion despite higher resistance.

The study underscores the critical influence of reservoir size and rebar configuration on corrosion dynamics. The larger reservoirs facilitate stable corrosion behavior by providing ample electrolyte availability, reflected in lower Rs and more consistent Icorr trends. In contrast, smaller reservoirs restrict ion mobility, leading to higher Rs and fluctuating but generally reduced Icorr values. The configuration of the rebar also plays a significant role, with three rebar systems demonstrating a greater propensity for active corrosion. This is attributed to increased electrochemical interaction and the larger cathodic area, which promotes localized anodic dissolution and accelerates corrosion processes.

Long-term observations reveal that environmental factors such as oxygen availability, moisture levels, and the degradation of the passive layer critically affect corrosion behavior. Notably, an increase in Icorr after 1400 days in several samples indicates the potential for renewed or intensified corrosion activity as protective mechanisms in the concrete matrix weaken over time. These findings have practical implications for infrastructure durability. To reduce rebar corrosion and extend the life of concrete structures, it's important to optimize reservoir size, keep environmental conditions stable, and use protective measures like corrosion inhibitors or better concrete mixes [30, 31].

## Conclusions.

The study of the corrosion behavior of fly ash concrete using the GP method highlights the significant role of environmental factors, reservoir size, and rebar configurations on corrosion dynamics. The variations in corrosion current over time demonstrate the complex interplay between oxygen availability, moisture content, and the integrity of protective passive layers. The findings reveal that these factors can cause significant fluctuations in corrosion activity, impacting the durability of reinforced concrete structures.

The reservoir size was found to be a critical determinant of corrosion behavior, with smaller reservoirs (2.5 cm) leading to higher variability in Icorr due to restricted oxygen and

electrolyte availability. The larger reservoirs (17.5 cm) exhibited more stable corrosion patterns, suggesting better support for corrosion kinetics. Notably, mid-sized reservoirs (7.5 cm) provided a balanced environment, offering moderate corrosion current values that reflect an equilibrium between oxygen diffusion and electrolyte presence. These results indicate that optimizing reservoir dimensions can effectively moderate corrosion processes.

The influence of rebar configuration was also pronounced, with three rebar systems displaying higher corrosion activity compared to single rebar systems. The increased surface area and electrochemical interactions in the three rebar configuration accelerated corrosion, as evidenced by more negative corrosion potentials and higher corrosion current values. Conversely, single rebar samples showed evidence of re-passivation, reflecting a less aggressive corrosion environment. The study's insights emphasize the need for a tailored approach in design and maintenance to enhance the durability of concrete structures, considering environmental and structural variables to mitigate corrosion risks effectively.

**Acknowledgements.**

The authors express their sincere gratitude to the Florida Department of Transportation (FDOT) for their support in sample preparation and acknowledge the financial assistance provided by FDOT and TriDurLE. Special thanks are extended to Florida Atlantic University (FAU) and the graduate and undergraduate students of the Marine Materials and Corrosion Laboratory at FAU for their invaluable contributions to laboratory work and data collection. The views and conclusions presented in this paper are those of the authors and do not necessarily represent the perspectives of FAU, FDOT, or TriDurLE.

**References.**

1. Angst UM (2018) Challenges and opportunities in corrosion of steel in concrete. Mater. Struct., vol. 51(4), pp. 1–20.

2. Jones AEK (1997) Development of a holistic approach to ensure the durability of new concrete construction. British Cement Association, Crowthorne.

3. fib-Model-Code (2010) 3rd FIP/CEB Model Code for concrete structures. Comite Euro-International du Beton and Federation International de Precontrainte.

4. Broomfield JP (2007) Corrosion of steel in concrete-understanding, investigation and repair, 2nd edition. Taylor & Francis, Oxford.

5. Ballim Y, Reid JC (2003) Reinforcement corrosion and the deflection of RC beams-an experimental critique of current test methods. Cement Concr. Compos., vol. 25(6), pp. 625-632.

6. El Maaddawy T, Soudki K (2007) A model for prediction of time from corrosion initiation to corrosion cracking. Cement Concr. Compos., vol. 29(3), pp. 168-175.

7. Liu Y, Weyers RE (1998) Modelling the time-to-corrosion cracking in chloride contaminated reinforced concrete structures. ACI Mater. J., vol. 95(6), pp. 675-681.

8. Malumbela G, Moyo P, Alexander MG (2009) Behaviour of reinforced concrete beams under sustained service loads. Constr Build. Mater., vol. 23(11), pp. 3346-3351.

9. Torres-Acosta AA, Fabela-Gallegos MJ, Munoz-Noval A, Vazques-Vega D, Hernandez-Jimenez JR (2004) Influence of corrosion on the structural stiffness of reinforced concrete beams. Corrosion, vol. 60(9), pp. 862-872.

10. Torres-Acosta AA, Navarro-Guitierrez S, Teran-Guillen J (2007) Residual flexure capacity of corroded reinforced concrete beams. Eng. Struct., vol. 29(6), pp. 1145-1152.

11. Fraay ALA, Bijen JM, de Haan YM (1989) The Reaction of Fly Ash in Concrete, a Critical Examination. Cement and Concrete Research, vol. 19, pp. 235-246.

12. Presuel-Moreno F, Balasubramanian H, Wu Y (2013) Corrosion of reinforced concrete pipes: an accelerated approach. Corrosion 2013, paper no. C2013-0002551 (Houston, TX).

13. Presuel-Moreno F, Nazim M, Tang F, Hoque K, Bencosme R (2018) Corrosion Propagation of Carbon Steel Rebars in High Performance Concrete. BDV27-977-08 Final Report for FDOT.

14. Andrade C, Alonso C (1996) Corrosion rate monitoring in the laboratory and on-site. Constr. Build. Mater., vol. 10(5), pp. 315-328.

15. Feliu V, Gonzalez JA, Feliu S (2007) Corrosion estimates from transient response to a potential step. Corros. Sci., vol. 49(8), pp. 3241-3255.

16. Gonzalez JA, Miranda JM, Feliu S (2004) Consideration on the reproducibility of potential and corrosion rate measurements in reinforced concrete. Corros. Sci., vol. 46(10), pp. 2467-2485.

17. Hoque K (2020) Corrosion propagation of reinforcing steel embedded in binary and ternary concrete. Ph.D. Dissertation, Department of Ocean and Mechanical Engineering, Florida Atlantic University (FAU), Boca Raton, Florida, USA.

18. Presuel-Moreno F, Hoque K (2019) Corrosion propagation of carbon steel rebar embedded in concrete. Corrosion 2019, Nashville, Tennessee, USA.

19. Otieno M, Beushausen H, Alexander M (2016) Chloride-induced corrosion of steel in cracked concrete-part I: experimental studies under accelerated and natural marine environments. Cem. Concr. Res., vol. 79, pp. 373-385.

20. O'Reilly M, Omid F, Darwin D (2019) Effect of Supplementary Cementitious Materials on Chloride Threshold and Corrosion Rate of Reinforcement. ACI Materials Journal, Title No. 116-M12, pp. 125-133.

21. Hoque KN, Presuel-Moreno F (2023) Accelerated Corrosion of Steel Rebar in Concrete by Electromigration: Effect of Reservoir Length and Concrete Mixes. Proceedings of the 13th International Conference on Marine Technology (MARTEC 2022).

22. Hoque KN, Presuel-Moreno F (2023) Corrosion Propagation of Steel Rebar Embedded in Marine Structures Prepared with Binary Blended Concrete Containing Slag. Proceedings of the 13th International Conference on Marine Technology (MARTEC 2022).

23. Hoque KN, Presuel-Moreno F, Nazim M (2023) Corrosion of carbon steel rebar in binary blended concrete with accel-

erated chloride transport. Journal of Infrastructure Preservation and Resilience, vol. 4(26), pp. 1-15.

24. Hoque KN, Presuel-Moreno F, Nazim M (2023) Accelerated Electromigration Approach to Evaluate Chloride-Induced Corrosion of Steel Rebar Embedded in Concrete. Advances in Materials Science and Engineering, Article ID. 6686519, pp. 1-14.

25. Presuel-Moreno F, Hoque K, Rosa-Pagan A (2022) Corrosion propagation monitoring using galvanostatic pulse on reinforced concrete legacy samples. 2020-FAU-02 Final Report for National University Transportation Center TriDurLE.

26. Hoque KN, Presuel-Moreno F (2023) Corrosion Behaviour of Reinforcing Steel Embedded in Fly Ash Concrete. Proceedings of the 13th International Conference on Marine Technology (MARTEC 2022).

27. Hoque KN, Presuel-Moreno F (2023) Corrosion of Steel Rebar Embedded in Ternary Blended Concrete Exposed to High Humidity Environment. Proceedings of the 13th International Conference on Marine Technology (MARTEC 2022).

28. Hoque KN, Presuel-Moreno F (2024) Electromigration-Based Investigation of Corrosion Behaviour in Ternary Blended Reinforced Concrete. International Journal of Structural and Civil Engineering Research, vol. 13(3), pp. 90-95.

29. Chao LC, Kuo CP (2017) Ternary Blends of High Aluminate Cement, Fly ash and Blast-furnace slag for Sewerage Lining Mortar. IOP Conference Series: Materials Science and Engineering, vol. 303(1), Article ID. 012023.

30. Johnson K, Garg A (2017) Partial Replacement of Wood Ash with Ordinary Portland Cement and Foundry Sand as Fine Aggregate. Journal of Civil and Environmental Engineering, vol. 7(2), Article ID. 1000272.

31. Hussain RR (2011) Underwater half-cell corrosion potential bench mark measurements of corroding steel in concrete influenced by a variety of material science and environmental engineering variables. Measurement, vol. 44, pp. 274-280.